Biophysical Journal Volume 105 December 2013 2820–2831

Structure and Mechanical Characterization of DNA i-Motif Nanowires by Molecular Dynamics Simulation

Raghvendra Pratap Singh,[†‡] Ralf Blossey,[‡] and Fabrizio Cleri[‡*]
[†]Institut d'Electronique Microelectronique et Nanotechnologie (IEMN UMR Cnrs 8520) and [‡]Interdisciplinary Research Institute (IRI USR Cnrs 3078), University of Lille I, Villeneuve d'Ascq, France

ABSTRACT We studied the structure and mechanical properties of DNA *i-motif* nanowires by means of molecular dynamics computer simulations. We built up to 230 nm-long nanowires, based on a repeated TC_5 sequence from crystallographic data, fully relaxed and equilibrated in water. The unusual $C{\cdot}C^+$ stacked structure, formed by four ssDNA strands arranged in an intercalated tetramer, is here fully characterized both statically and dynamically. By applying stretching, compression, and bending deformations with the steered molecular dynamics and umbrella sampling methods, we extract the apparent Young's and bending moduli of the nanowire, as well as estimates for the tensile strength and persistence length. According to our results, the i-motif nanowire shares similarities with structural proteins, as far as its tensile stiffness, but is closer to nucleic acids and flexible proteins, as far as its bending rigidity is concerned. Furthermore, thanks to its very thin cross section, the apparent tensile toughness is close to that of a metal. Besides their yet to be clarified biological significance, i-motif nanowires may qualify as interesting candidates for nanotechnology templates, due to such outstanding mechanical properties.

INTRODUCTION

Among the nonstandard DNA structures constructed from basepairs not following the standard Watson-Crick (WC) association rule, the i-motif is the most recently identified (1–3). Its existence has been assessed in vitro, under acidic pH conditions, as a tetrameric structure formed by four intercalated DNA strands, held together by protonated cytosine-cytosine, or $C{\cdot}C^+$, pairs. However, i-motif tetramers as well as G-tetraplex have also been observed in vivo (4,5), most notably in the terminal part of the human genes, or telomere, where rather long (50–210 bases) asymmetric G-rich and C-rich single-stranded portions of DNA are found. At present, it is not yet clear whether such DNA tetraplex structures are stably formed and used by eukaryotes, although the duplex-tetraplex interconversion has been studied in some details (3). From such studies it was observed that at physiologic conditions of pH, salt concentration, and temperature, the C-rich and G-rich strands form a normal WC duplex, whereas at pH between 4.5 and 5 the i-motif and the G-quadruplex become the most stable and abundant forms of supramolecular association.

The stabilization of poly-C DNA strands upon lowering the pH, and the resulting $C{\cdot}C$ pairing, has been attributed to the hemiprotonation of the C bases (6,7). One extra hydrogen bond is formed when a proton is resonantly exchanged between the two facing N atoms of the basepair (Fig. 1 *a*), now a $C{\cdot}C^+$, which leads to stabilization of such a non-WC structure. Hemi- (or resonant) protonation of C bases is clearly characterized by two Raman lines at 1385 and 1542 cm^{-1} (8), whereas the resulting tetrameric arrangement of the sugar-phospate backbone (Fig. 1 *b*) with its unique stacking, can be recognized by the fingerprints at 804, 852, 888, and 972 cm^{-1} (8).

The identification of the elementary process of resonant protonation above led to the suggestion of possible i-motif formation pathways, which were experimentally tested on extended C-rich nanowire tetrameric structures formed by C_7 (8), C_7GC_4 (9), and TC_n ($n = 3,4,5$) (10) base motifs. Notable information that emerges from such studies is that the formation of the tetrameric stacked structure should not proceed through association of preformed dimers, but rather by fast, successive intercalation of single strands into short-lived dimer and trimer species. The fact that $C{\cdot}C$ dimers are not observed to compete with the tetramers at low enough pH shows that the C-rich dimer is fairly unstable on the timescale of the tetramer association reaction. In the following we will demonstrate by our molecular simulations that this is indeed the case.

The stability of the tetrameric nanowire structure is found to increase rapidly with the number of $C{\cdot}C^+$ pairings per unit, as shown in (10), the lifetime (in minutes) of TC_n tetramers, obtained by NMR NOESY and TOCSY spectra, increasing by about two orders of magnitude for each unitary increase of n.

From a theoretical point of view, atomistic simulations (11–13) indicate that the stabilization energy of the $C{\cdot}C^+$ pairing indeed results from a subtle balance between the increased electrostatic repulsion of the PO_4 groups, closer in the tetramer than in standard dsDNA; favorable dipolar interactions between the C-N and C-O dipoles in stacked pairs; and the extra dipolar interaction plus H-bond energy, induced by the resonant protonation of $N^{\cdots}N$ atoms of the facing cytosines. Recent molecular dynamics (MD) simulations (14,15) confirmed the stacking structure, and

Submitted June 24, 2013, and accepted for publication October 8, 2013.
*Correspondence: fabrizio.cleri@univ-lille1.fr
Editor: Nathan Baker.

0006-3495/13/12/2820/12 $2.00
http://dx.doi.org/10.1016/j.bpj.2013.10.021

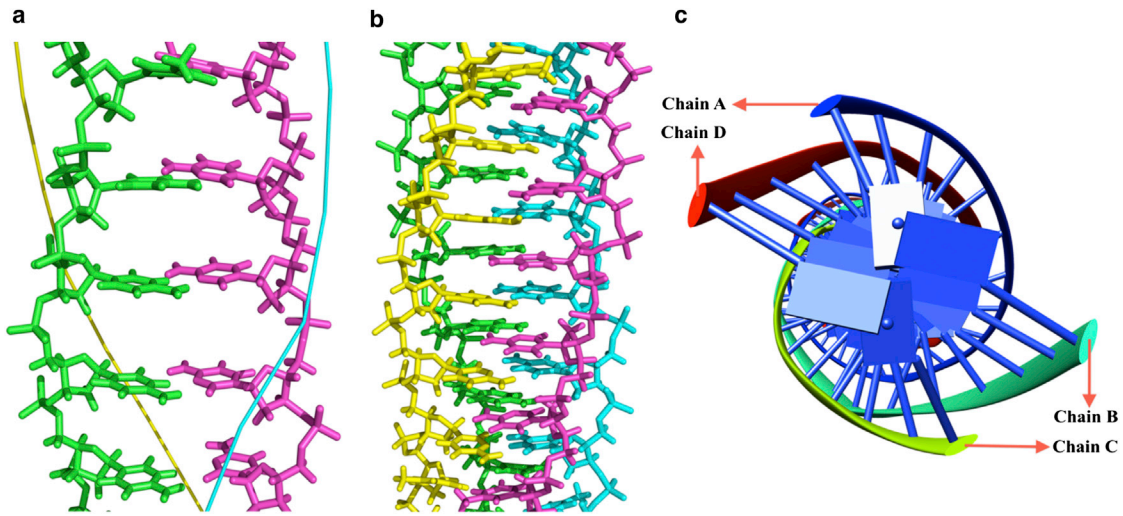

FIGURE 1 (*a*) Side view of the n[d(TC_5)] basic dimer in stick representation, with the two chains colored differently, as obtained from the crystallography-resolved structure and duplicated n times. (*b*) Side view of the n[(TC_5)$_4$] intercalated tetramer, used as a starting configuration for MD simulations. The intercalated yellow-cyan chains are identical to the green-magenta pair, rotated by ~50° and shifted by 0.31 nm about the z axis. (*c*) Top view of the intercalated tetramer in a different graphical representation, showing the double-grooved secondary structure. To see this figure in color, go online.

underscored the role of sugar-sugar interactions along the backbone as a further stabilizing element.

In addition to their possible role in the genome, still awaiting a full clarification, such DNA nanowires can be also attractive in the domain of bioinspired materials for nanotechnologies. Notably, various kinds of biomimetic nanowires have been already obtained from B-DNA (16), proteins (17), and even from viral particles (18). Electrical, optical, plasmonic features have been added to such wires by metallization, wherein metals have been coated or molded onto the outer or inner surfaces of these biomolecular templates (19–21). The i-motif could as well be a good candidate for nanotemplating, being easily manipulable and apparently stable over quite long timescales (8). However, although its structure is rather well assessed, a thorough mechanical characterization of such bionanowire is still lacking, and even such basic quantities as the persistence length have not been described yet. One of the main results of this study will be to shed light on such important mechanical features.

In this work, we studied the mechanical properties of i-motif nanowires by means of all-atom MD computer simulations. We built very long tetramers, up to 230 nm, based on the TC_5 base unit embedded in a shell of water with appropriate counter ions. We made use of several computational techniques based on molecular constraints, as well as the steered MD (SMD) (22,23) and umbrella sampling (24) methods, to simulate the application of external forces to the i-motif. According to the eigenmode of deformation, we extract the equivalent Young's modulus, toughness, bending stiffness, and hence the persistence length of the nanowire. We compare our results to the corresponding data for dsDNA with the same base sequence, and to several other biopolymers. Finally, some biological and nanotechnology implications of our findings are discussed.

MATERIALS AND METHODS

We constructed the atomistic model of the *i-motif* from the NMR crystallographic structure of (TC_5)$_4$ tetramer, resolved by Gehring, Leroy, and Guéron (1) (PDB id: 225D). Hydrogen atoms were added to the topology following the Charmm27 force field guess method. The extra proton on N3 of cytosine was added, with initial orientation adjusted according to the experimental indications (10).

According to the suggestions of Leroy et al. (2,10), protonation of the N3 atom of cytosine, necessary for the formation and stability of this supramolecular structure could be realized in a few different ways: i), cytosines belonging to adjoining strands are alternately protonated along the ladder; ii), two out of four strands are completely protonated at N3 of cytosine, whereas the two others carry the usual cytosine nucleotide; iii), the charges (proton of N3) are situated around, and separated by, the narrow groove; iv), the charges are situated around, and separated by, the wide groove of the i-motif. From all of these possibilities we have chosen the second one, namely to start from a structure with two nearby chains fully protonated, although the other two were normal cytosine nucleotides. This choice was motivated because we wanted to check the possibility of protons dynamically jumping from one chain to the other, as well as the implementation of modified force field parameters. In fact, it turned out to be easier to implement a new set of parameters for just two of the chains, whereas using the normal force field parameters for the other two, rather than a new set of hybrid parameters for all the four half-protonated hybrid chains.

Energy minimization of the isolated structure at constant volume was first carried out with the NAMD software (22). The structural energy of the system was again minimized after diluting the molecule in water, where the maximum compactness was attained, and an extra hydrogen bond was formed between the C•C pairs. We used the TIP3P water model in all of our simulations. The hydrated structure of the fragment with a length $L = 3.6$ nm, was subsequently used as the basic unit for all the foregoing input structures and simulations. Initial structures for longer fragments n[(TC_5)$_4$] were constructed by translating $n = 4$, 8, 16, 32, or 64 times the basic unit coordinates along the z axis of the optimized

geometry of the relaxed $(TC_5)_4$ unit. Chimera (26) and VMD (27) molecular modeling packages were extensively used in this stage, also to generate the missing terminal residues (P, O1P, and O2P), which are the essential backbone atoms participating in the formation of the phosphodiester bonds to join the prime (3′ and 5′) ends of the previous nucleotide with the next in-line along the backbone. In this way, we generated i-motif structures up to ~230 nm length for the $32[(TC_5)_4]$.

We performed finite temperature MD simulations at T = 300 K, of: i-motif DNA tetramers of different lengths, both with protonated and nonprotonated C•C pairs; a dimer with 8 basic units ($L = 28.8$ nm) and the same sequence, i.e., $8[(TC_5)_2]$ (akin to a dsDNA with a $8\times(dTC_5)$ sequence); and on a single strand of i-motif monomer of the same length, i.e., $8[(TC_5)]$ (akin to a ssDNA with a $8\times(TC_5)$ sequence). For each of these systems, we initially performed a fully restrained minimization (i.e., with the DNA fragments immobile) in a large box of TIP3P water with XYZ size of $9 \times 9 \times (L+6)$ nm^3, and ions at 0.2 mM/l, to let water and ions to settle at their optimum starting positions. Subsequently, a position-restrained minimization of the system was performed, with restraints still applied on the phosphodiester quadruple backbone of the i-motif. Eventually, we ran all-atom unconstrained minimization under constant-{NPT} conditions, followed by quenching to obtain the best starting structures with the lowest energy at T = 0 K. Finite-temperature equilibration runs at T = 300 K and constant-{NVT} were subsequently performed for 2 ns. From such well equilibrated starting structures we launched the actual production runs, of duration 5 up to 10 ns, saving the atomic coordinates every 1 ps. In this way, 5 to 10,000 frames per each simulation were recorded. A summary of the main simulations carried out is given in Table S1, in the Supporting Material.

SMD simulations were performed, to study the elasticity under stretching and bending of the hydrated i-motif structures, using the constant-velocity or constant-force protocols of NAMD. To perform SMD, we kept fixed either four atoms (for i-motif tetramers), or two atoms (for i-motif dimers) at one end of the structure. Similarly, at the opposite end, four or two atoms, called SMD atoms, were selected to carry the applied constant velocity. Under the applied perturbation to the SMD atoms at one end, while holding still the fixed atoms at the other end, the i-motif structure responds by developing a steady deformation, tension, compression, bending, according to the eigenvector of the applied perturbation.

Such SMD simulations were performed for all of the four-, double-, and single-stranded i-motif structures described previously. The center of pull was calculated by averaging the coordinates of all the SMD atoms. The direction of pull was identified by the direction of the vector connecting the fixed and SMD atoms. In practice, the center of pull of the SMD atoms was attached to a dummy atom by a virtual spring (22,23). The constant velocity along the z-coordinate axis was applied to the dummy atom and the force was measured between dummy and SMD atoms. After several tests, a virtual spring constant of 1 kcal mol^{-1} Å^{-2} was adopted (1 kcal mol^{-1} Å^{-2} = 695 pN nm^{-1}) together with typical pulling speeds of 1–3 ms^{-1}, to ensure a reasonable signal/noise ratio.

Bending was also simulated by means of the umbrella sampling technique (24). We used a harmonic biasing potential, only to simulate the action of a force at the midpoint of the nanowire (the central nucleotide tetrad, one base per chain), while holding still the two extremes. In this way we could drive the nanostructure along the bending deformation trajectory, with a pulling velocity of 5 ms^{-1} up to reaching the maximum deformation of 5 nm. The umbrella potential provided the confinement in the required deformed structure, while further relaxation steps were performed to explore the most stable conformations and to extract the corresponding values of deformation energy and force along the trajectory.

RESULTS

Molecular structure characterization

Because we started by rigidly duplicating a small portion of i-motif tetramer, namely a tetrameric fragment obtained from the x-ray crystallographic structure, we found it necessary to compare the equilibrated structures of all our i-motif systems, both protonated and nonprotonated, as well as the dimer with the same sequence, to gain better insight into the structural features and dynamical stability of our systems. In Fig. 1 we show: (*a*) the structure of the relaxed, protonated dimer, with a repeated $[(TC_5)_2]$ (or equivalently, $d(TC_5)$) structure; (*b*) a side-view of the relaxed, protonated i-motif tetramer, $[(TC_5)_4]$, formed by intercalation of two identical $[(TC_5)_2]$ dimers; and (*c*) the top view of the same tetramer.

From the crystallographic coordinates of the i-motif basic unit, the average interplanar distance between adjacent cytosines along a same chain is 0.62 nm, whereas the intercalating distance between adjacent cytosines belonging to different chains is 0.31 nm (see Fig. 2 for a *definition of such distances*). Therefore, the nucleotides in each single chain (out of four in the i-motif) have larger distances than their classical B-DNA counterpart. This agrees with the difference in contour length L between the i-motif and a B-DNA with the same nucleotide number and sequence (in fact, 50 bp correspond to $L = 16.3$ nm in B-DNA, and $L = 28.85$ nm in the i-motif). After the full-energy optimization, the T = 0 K relaxed i-motif structures attained an average interplanar distance of 0.64 nm between the nucleotides of the same chain, or basepairs of the parallel pair of chains (the dimer), whereas the average intercalating distance settled to 0.32 nm, close to the stable value of B-DNA. The two intercalating dimers are antiparallel to

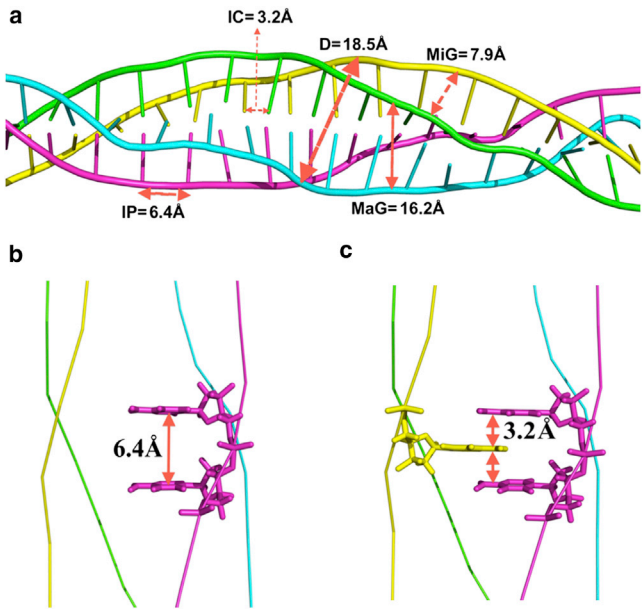

FIGURE 2 Definition of the various distances of the nucleotides in the four chains composing the i-motif tetramer. Average values obtained after the relaxation-equilibration MD cycle described in the text. (*a*) IP = interplanar (or base stacking) distance (see also (*b*)); IC = intercalation distance (see also (*c*)); D = diameter; MiG = minor groove width; MaG = major groove width. To see this figure in color, go online.

each other, arranged like the 5′-3′||5′-3′ and 3′-5′||3′-5′ ordinary DNA duplex. Such structural data agree with previous calculations by Malliavin et al. (15).

In B-DNA with random sequence, the interplanar distance on both strands is ~0.34 nm, whereas in each of the two dimers making up the i-motif it is ~0.64 nm. This means that each dimer composing the i-motif is much less twisted than B-DNA: indeed, we measure an average twist angle of ~12° compared to ~34° in B-DNA, with a correspondingly higher helical rise per basepair. However, it should be noted that in the experiments (1,7,9) dimers are very short lived and either decay back to monomers, or directly evolve to tetramers by some yet to be clarified mechanism.

It is also worth noting that the i-motif structure displays a minor and a major groove (see Fig. 1). However, this nomenclature must not be confused with the corresponding features of B-DNA, in which the tertiary structure (the *helical folding*) gives rise to two grooves. In the i-motif, the two grooves are both due to the secondary structure of the strands whose intercalated pairs are rotated by ~50° about the common z axis (Fig. 1 *c*), thus defining two sets of average distances between the P backbones, (Fig. 2 *a*).

The large interplanar distance in the dimer which, as said, means a larger basepair rise as well as smaller tilting angle, sliding and bending parameters per basepair, should make in principle the *i-motif* structure stiffer and more straight compared to B-DNA. The average diameter is $D = 1.85 \pm 0.05$ nm, calculated by assuming an average cylindrical shape delimited by the backbone P atoms of the four chains. It is worth noting that such a less twisted, straighter structure makes the i-motif also thinner than B-DNA, despite being formed by twice as many nucleotides, with a resulting nearly doubled atomic density. The more detailed structure analysis shows that the diameter differs between cytosine-rich regions and intercalated thymine tetrads. By calculating the average distance between the N3 atoms of facing nucleotide pairs from the four chains, an inner cylindrical region of the nanowire can be also identified, with a diameter of $D_i = 0.35 \pm 0.03$ nm.

Dynamical stability

The sugar pucker of the ribose ring is an important feature indicating the helical shape of the backbone. In nucleic acids the sugar pucker is responsible for their helical nature. The five-membered ring of the ribose sugar cannot be planar because of steric reasons, therefore one or two atoms move typically by 50 PM above (endo) or below (exo) the plane of the sugar ring. In DNA, the C2′-endo and C3′-endo conformations are found to be in equilibrium, and help DNA to acquire its normal B-form, whereas a predominance of -exo conformations would rather push the DNA to acquire the dehydrated A-form. On the other hand, RNA molecules strictly follow C3′-endo sugar pucker.

In our thermally equilibrated i-motif structures we always observed the C3′-endo configuration (i.e., the carbon C3′ moves above the plane C1′-O4′-C4′) for all cytosine pairs, including the thymine nucleotides at the 5′ terminus, except the 3′-terminal cytosine, which was found to switch dynamically between C4′-exo and C3′-exo sugar pucker. We also observed a temporary switching to the C4′-endo for some nucleotides, a relatively rare event during very long MD trajectories.

The next important indicator in the stabilization of the i-motif structure is the conformation of thymine nucleotide tetrad (i.e., the layer where the four Ts from the four intercalating chains meet). Experimental studies show that in this tetrad of thymines, one of the pairs is always hydrogen bound and paired, whereas the second pair could either bind inward, or extend outward from the cylindrical core structure (29). Interestingly, after MD relaxation we found some thymine tetrads (i.e., a layer of T bases, separated by five C tetrads, in the repeated (TC_5) four-stranded structure) behaving exactly in this way. Typically, we observed one thymine tetrad with an extended outward pair (see *arrows* in the next Fig. 3 *a*), alternating to a nearby tetrad with all four T's inward bound and properly paired.

To demonstrate the stabilization of the structure ensured by the protonation, we compared the dynamical evolution of the fully protonated 8[$(TC_5)_4$] i-motif and the nonprotonated (*np*) tetramer with the same nucleotide composition,

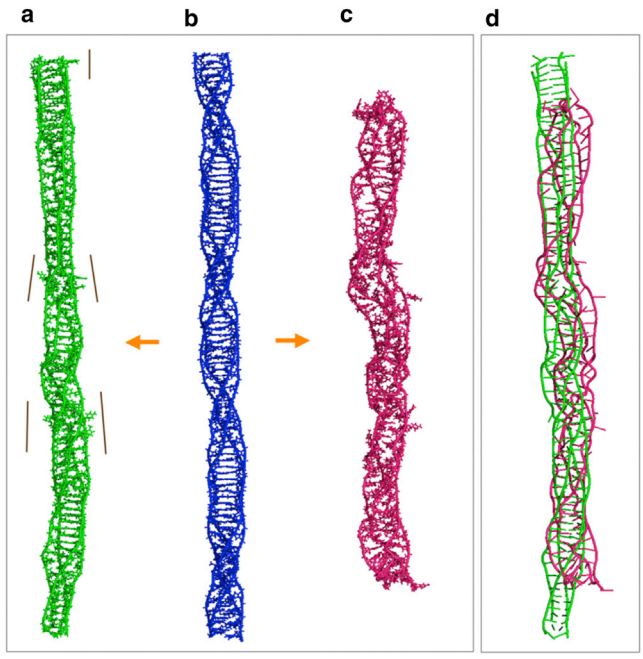

FIGURE 3 Comparison of the structure of the protonated versus nonprotonated i-motif tetramer after 5 ns of MD at T = 300 K. The central (*b*) structure in blue is the initial configuration, identical for both cases; (*a*) the protonated i-motif tetramer (*thin bars indicate the outward leaning thymines*); (*c*) the nonprotonated tetramer structure; (*d*), the two structures superimposed. To see this figure in color, go online.

$8[(dTC_5)_2]$, over a timescale of 5 ns (in practical terms, the two starting structures were identical, apart from the extra proton). In Fig. 3 we show a comparison of the structures of the i-motif (*a*) and the *np*-tetramer (*c*), starting from the same, unrelaxed 8-unit configuration (*b*). We find that during this time the *np*-tetramer crumbles, and loses its i-motif-like initial structure, becoming a rather disordered structure with different interplanar distances for every basepair. In Fig. 4 we also show, for better clarity, only one chain each for the i-motif (*a*) and the *np*-tetramer (*b*), in each case comparing the instantaneous conformation of the chain after 5 ns of MD, against the initial unrelaxed structure. For the *np*-tetramer, the backbone turns from a nearly straight wire to a somewhat helicoidal form, and the core of the structure is destroyed. By contrast, the protonated i-motif maintains a linear and straight backbone, with constant interplanar and intercalation distances, eventually adjusting to the final stable straight conformation and reorganizing the initial defects introduced by the artificial periodic construction. We calculated the solvent accessible surface area (SASA) by the modified version of the Connolly algorithm available in VMD, using a spherical probe radius of 1.4 Å and averaged over 500 samples. It was observed an increase of the specific SASA by ~20%, going from the value of 27.8 nm^2 for the stable 8-units i-motif, to 33.25 nm^2 for the disordered tetramer. Such a huge increase clearly indicates a much more open structure of the disordered, nonprotonated i-motif. All the findings clearly support the idea of the importance of protonation, in establishing the form and integrity of the i-motif structure.

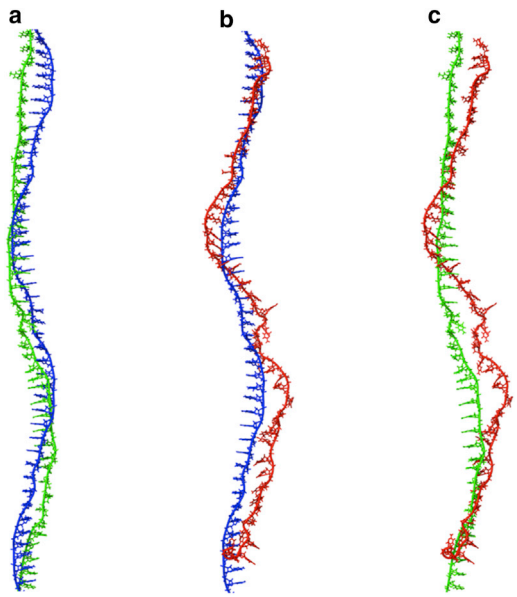

FIGURE 4 Comparison of the structure of the protonated versus nonprotonated i-motif tetramer (*snapshot of one chain from each tetramer*) after 5 ns of MD at constant-{NVT}. The blue chain is the first time step, identical for both simulations; (*a*) the green chain is the protonated i-motif; (*b*) the red chain is the nonprotonated tetramer with the same nucleotide composition; (*c*) protonated (*green*) and nonprotonated (*red*) chains superimposed. To see this figure in color, go online.

Because the two identical $n[(TC_5)_2]$ dimers are intercalated, each T•T and C•C+ pair of hydrogen-bonded nucleotides (at the average distance of 0.62 nm) from one dimer, will have either a T•T or a C•C+ pair from the other dimer, as a nearest neighbor (at the average distance of 0.32 nm). Therefore, in our i-motif tetramer, there are three different sets of tetrads, formed by adjacent basepairs from different dimers: a purely C•C+ tetrad; a purely T•T tetrad; and a mixed C•C+/T•T tetrad. Although the overall behavior of the structure is conserved during the dynamics, these tetrads follow a slightly different behavior in their respective local environment. The C•C+ tetrad shows a high degree of compactness, and the distances between inter- and intrabackbone P atoms are within the experimental ranges. For the i-motif the interstrand P distance is 0.79 nm (NMR value 0.76 ± 0.03 nm (28)) and intrastrand P distance is 1.53 nm (NMR value 1.54 ± 0.03 nm (28)).

The behavior of the T•T tetrad is different. One pair of thymine nucleotides from facing chains is paired by using the two available hydrogen bonds and remains inside the cylindrical geometry. The other two Ts from the two other facing chains, can move away from the cylindrical geometry, thus leaning outward from the core structure (*thin bars* in Fig. 3 *a*). Such an outward displacement forces also the neighboring cytosines (which are also part of the mixed C•C+/T•T tetrad) to deviate from the compact cylindrical arrangement. Notably, this results in larger P-P distances at the T•T site and a locally wider groove architecture (25).

Water and ions distribution

Positioning of the water molecules in closeby solvation shells is another very important factor in stability and functionality of nucleic acids in their cellular environment. Hence, we also studied the water and ion concentration around our *i-motif* structures. The average density of water molecules and ions per unit volume as a function of the distance from the nanowire surface are shown in Figs. 5 and 6, respectively; a typical cross section of thickness 6 nm along *z* is shown in Fig. 7. We find that water molecules closer to the i-motif surface tend to penetrate the major groove (*green region* in Fig. 7), whereas they align along, but not inside, the minor groove of the *i-motif* (*orange region*). Such an apparent hydrophobic behavior of the minor groove limits the solvent accessibility (2), which in fact attains the normal STP water density only at ~0.6 nm away from the outer surface of the nanowire (Fig. 5). This effect reduces the backbone repulsion, with an overall stabilizing effect on the i-motif structure. It is worth noting that in the case of B-DNA, water is known to have cooperative effects on binding of ligands and DNA binding proteins (29), although in

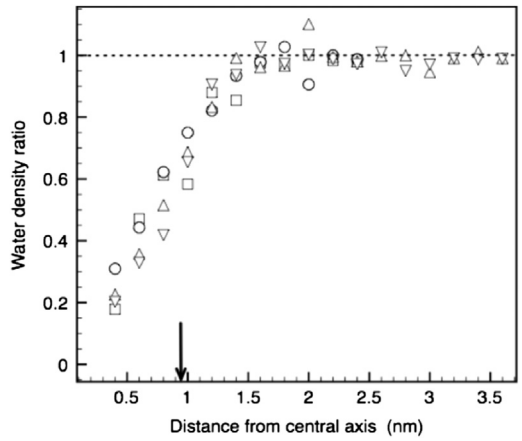

FIGURE 5 Radial density of water molecules around the i-motif nanowire, expressed as a fraction of the normal density at STP. The zero of the abscissa corresponds to the central z axis. The arrow indicates the outer i-motif surface (*approximate radial position of the P backbone*). Symbols are averages over axial slices of 6 nm, taken at different positions along the axis.

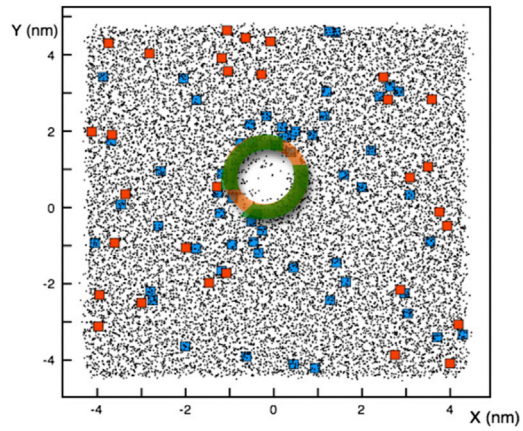

FIGURE 7 Cross section (9×9 nm^2) of the water molecules (*dots*), Na^+ and Cl^- ions (*blue* and *red squares*), in a thickness of 6 nm along the z axis in the central portion of the nanowire, projected in the xy-plane normal to the cylinder axis. The thick circle indicates the average position of the i-motif major groove (*green*) and minor groove (*orange*). To see this figure in color, go online.

the case of the i-motif the minor groove shows a rather high degree of hydrophobicity.

On the other hand, the radial distribution of counter ions about the i-motif phosphate backbone in Fig. 6 is in qualitative agreement with the shape of the radial distributions generally observed for B-DNA (30). Notably, Na^+ ions tend to cluster around the PO_4^- backbone groups, in this case mostly around the (more hydrophobic) minor groove with a noticeable subsurface peak of ~0.3 mM/l (see also Fig. 7). Around the nanowire we find a concentration of ~0.7 mM/l, within a distance of 1 nm from the surface. Conversely, Cl^- ions are nearly absent up to a large distance from the surface, with just a small peak at 1 nm at a concentration ~5 times smaller than Na^+; a similar effect is observed in B-DNA, however with a larger ratio of ~10 between positive and negative counter ions (30). After ~1.5 nm, the Cl^- concentration settles to the same constant value of 0.17 mM/l, similar to Na^+ at the same distance, ensuring a neutral solution on average.

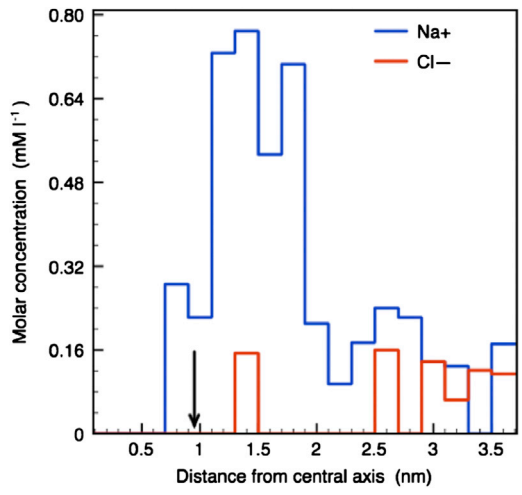

FIGURE 6 Radial molar density of Na^+ (*blue*) and Cl^- ions (*red*) around the i-motif, averaged over the entire nanowire length. To see this figure in color, go online.

Uniaxial stretching modulus

The elastic behavior of biomolecules under uniaxial deformation has been studied experimentally by a variety of techniques, such as optical or magnetic tweezers (see e.g. (31)), or atomic force microscopy (AFM, see e.g. (32). and references therein). After a number of phenomenological studies mainly aiming at the interpretation of the experimental data, the theory behind such experiments is by now pretty well understood (see e.g. (33–35).), also highlighting the correspondence between different experimental conditions, and between polymers with widely different molecular structures (36–38).

At a more microscopic level, molecular simulations have been extensively and successfully used to estimate the elastic moduli of various biomolecules, covering a wide spectrum of situations (see (39) and references therein). In our MD simulations, we calculate first-order elastic coefficients within the framework of linear elasticity. To bypass the entropic elasticity regime, we started from a fully extended nanowire along the axial direction, with contour length $L = 28.8$ nm as the reference state. Next, we applied the tensile deformation along the nanowire axis (see Materials and Methods). Because we had no prior knowledge about the possible range of values of the stretching modulus, the most critical step in such a computer experiment was to choose the right combination of pulling velocity and spring constant for the spacer spring (between the set

of dummy atoms and the pull group). The main problem is that, for linear elasticity to be valid, one has to remain in a regime of extremely small deformations, which, in a complex molecular structure makes for a very noisy estimate of a fluctuating force at fixed small displacements. We tried various combinations of spring constant and pull velocity, and finally we settled upon a spring constant of 1 kcal mol^{-1} $Å^{-2}$ or ~0.7 Nm^{-1} (comparable to an AFM tip) and pulling velocity of 1 ms^{-1} (in fact, much faster than any experiment), which ensured a reasonably slow and steady response of the nanowire.

Fig. 8 shows the typical result of a uniaxial deformation experiment, both in compression and in tension. The force-displacement plot under such conditions is indeed quite noisy and displays a moderately oscillatory shape due to the nonhomogeneous (also in time) relaxation. However, it should be noted that the relative elongation $\Delta L/L$ over which we compute the elastic modulus is extremely small, for a typical MD simulation (see *ordinate axis* in Fig. 8), therefore the amplitude of force fluctuations appears larger on this scale. In the approximation of the nanowire as a linear-elastic rigid rod of uniform density, the Young's modulus Y is the coefficient relying on the force per unit area to the relative elongation. Therefore, it can be extracted from the linear fit of the f vs. ΔL data in Fig. 8, as

$$\frac{f}{A} = Y\left(\frac{\Delta L}{L}\right), \tag{1}$$

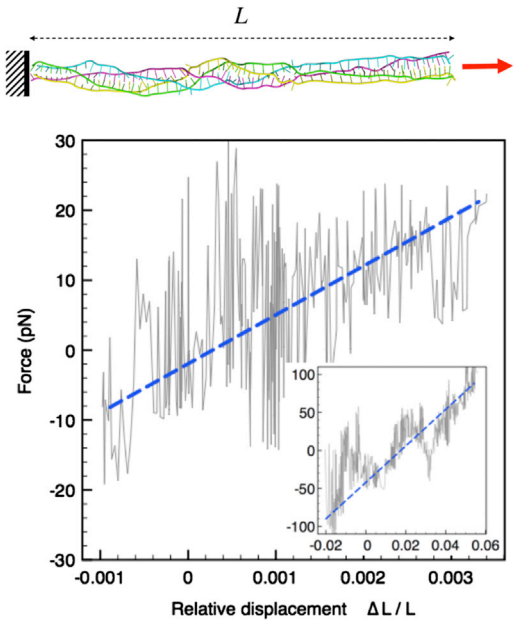

FIGURE 8 Force-displacement plot for uniaxial stretching deformation of the i-motif tetramer, for a constant pulling velocity of 1 ms^{-1} and a spacer spring constant of 1 kcal mol^{-1} A^{-2}. Top: scheme of the bending simulation. The thick dashed line is the linear fit to the average mechanical response. The inset shows a simulation with pulling velocity of 5 ms^{-1} and spring constant of 7 kcal mol^{-1} A^{-2}. To see this figure in color, go online.

with A the cross section of the nanowire (assumed cylindrical), defined by the previously estimated value of average radius $R = 0.95$ nm. From the best fit, we estimate $Y = 1.8 \pm 0.5$ GPa, a quite large value compared to that of B-DNA, which lies rather in the range of 0.35 GPa (40). For the sake of comparison, the inset of Fig. 6 shows the results of a run with a larger spring constant of 7 kcal mol^{-1} $Å^{-2}$ and pulling velocity of 5 ms^{-1}: for this case we obtain a Young's modulus about half the previously estimated value. Such a softening is a clear signature of the too large (i.e., too rigid) spring constant, also leading to wider force oscillations.

We probed the nanowire toughness in stretching well beyond the linear elastic regime, without detecting any signs of mechanical instability up to forces of the order of 1000 pN and more. This would correspond to a tensile strength exceeding 300 MPa, notably as good as a mild steel or aluminum alloy wire. Also in this respect, the i-motif appears to differ substantially from B-DNA, which is known to undergo a kind of structural, or melting transition above a tensile force of ~65 pN (40) (a fact that also complicates the direct measurement of Y).

Bending stiffness

Experimental measurements of the bending rigidity of polymers are based on variants of either one of two, quite general approaches: i), exploit the dependence of thermal fluctuations on the stiffness, or ii), measure the force needed to actively bend the polymer. In the first approach, the fluctuations of free filaments are monitored as a function of wavelength by light microscopy (also called flicker spectroscopy (41)). The second approach is typically implemented by measuring the force needed to push, e.g., by an AFM tip, a single filament deposited on a nanoscale patterned surface (42–44), in analogy with a macroscopic three-point bending measurement.

Both such experimental techniques can effectively be mimicked by MD simulation (45). The second one is but a variant of the tensile experiment described in the previous section, the force being applied at the center of the polymer while the two extremes are held fixed. The free fluctuation, however, is more complicated to observe on the MD timescale, because it requires that either i), the contour length of the simulated polymer be much longer than its persistence length, or ii), the simulation time be long enough with respect to the longest-wavelength fluctuation relaxation time, this being in turn inversely proportional to the lowest frequency and, therefore, directly proportional to the contour length.

In fact, we tried to observe the free fluctuation of our longest *i-motif* nanowire (230 nm) during quite long, constant-{NVE} MD simulations. However, even for simulation times exceeding 10 ns, the nanowire remained

practically straight, suggesting that its persistence length should be at least in the few hundred nm range.

Therefore, we had to resort to the direct deformation by a simulated three-point bending experiment. Instead of the SMD, we found it more practical to use the umbrella sampling feature of NAMD (24), to smoothly move the i-motif along the bending trajectory, while recording the force at the midpoint. We fixed both the prime ends of the i-motif with contour length $L = 28.8$ nm, by using a harmonic constraint on the four terminal C atoms. We then selected the midpoint (the 24th nucleotide of each chain) and with the umbrella potential we pulled at constant velocity this set of four nucleotides along the x axis (perpendicular to the main z axis of the nanowire), up to reaching a maximum displacement of about $\delta = 5$ nm (see Fig. 9, *top panel*). We had to adjust the water box size, because the lateral extent of the bent structure exceeded the standard box dimensions, thereby starting to experience interaction with its periodic image.

While pulling the central nucleotide every time the displacement δ had increased by 1 nm we stopped the simulation, fixed all three extremes of the *i-motif* (end-groups and pull-group) using harmonic constraints, and equilibrated the bent structure under constant-{NPT} for 5 ns, at P = 1 atm and T = 300 K. After such an equilibration step, the bending deformation would also add a variable amount of stretching, up to a maximum of ~2 nm for the maximum bending of 5 nm. Therefore, to get back to a contour length as close as possible to that of the initial structure and get rid of excess deformation energy, we performed a cycle of end-to-end compression for ~1 ns, during which the length was adjusted until the residual extension/compression was within $\pm 0.3\%$. This compression step was followed by another constant-{NPT} equilibration cycle of ~2 ns. After such an equilibration procedure, the umbrella sampling simulation was restarted, until the next increase of δ by another 1 nm was reached, and so on. In Fig. 9 we plot the overall force versus displacement curve, the latter being measured at the central (pull) group, together with a scheme showing the geometry of the simulated bending experiment. It could be noted that the f versus δ curve shows a kind of step-like shape, due to the alternating bending and relaxation procedure described previously.

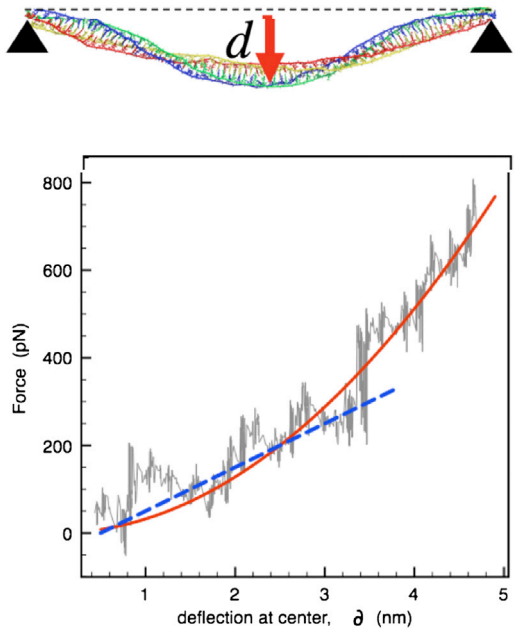

FIGURE 9 Force-displacement plot for bending deformation of the i-motif tetramer. Top: scheme of the bending simulation. The red continuous line is a guide to the eye (*quadratic fit*); the thick-dashed blue line is the best linear fit. To see this figure in color, go online.

If the i-motif nanowires were homogeneous and isotropic, the bending stiffness would be easily obtained from the Young's modulus as $B = Y \cdot I$, with I the second moment of the transverse cross section, which, for a homogeneous cylinder of radius R, would be $I = (\pi/4)R^4$. From this simple relationship we get an estimate of $B = 1.7 \cdot 10^{-27}$ N m^2.

A better estimate can be obtained from the calculation of the displacement δ at the midpoint produced by a point load f, as the derivative of the elastic energy with respect to the load (beam theory, Castigliano's theorem (46)):

$$\delta = \frac{\partial}{\partial f}\left(\int_{-L/2}^{L/2} \frac{M^2(l)}{2\,B}\,dl\right) = \frac{f\,L^3}{48\,B}, \tag{2}$$

l being a variable spanning the contour length L, and $M(l) = (1/2)f \cdot l$ the bending moment, assumed to be linear along the contour length for a straight bar. From our force plot as a function of δ in Fig. 9, we can therefore get the following estimate for the bending stiffness:

$$B = \frac{\alpha\,L^3}{48}, \tag{3}$$

with $\alpha = 0.062$ N m^{-1} the linear slope of the $f(\delta)$ curve in Fig. 9 (*dashed line*), resulting in $B = 2.6 \pm 0.4 \cdot 10^{-26}$ N m^2, considerably larger than the simpler previous estimate.

We note that Eq. 2 neglects any shear effects in the wire, which, at the molecular scale, would manifest as small rearrangements of the bases about the backbones of the four intercalated chains. Moreover, using a constant B value in Eq. 2 implies the same previous geometric homogeneity approximation, for the second moment I. Furthermore, some residual elastic energy from stretching and/or compression remains in excess (numerically estimated at $<1\%$) after each equilibration. However, all such uncertainties are within the (conservatively large) quoted error bar.

Persistence length

In our first attempts at studying the free fluctuation of the i-motif nanowire we wanted to use the fluctuation data also to extract the persistence length λ_p. As previously mentioned, such an attempt was frustrated by the quite high bending rigidity observed. It is worth noting that, from a statistical mechanics point of view, λ_p has the meaning of a correlation length, expressing the distance over which the expectation value of the tangent between any two points along the contour length L of the polymer, becomes exponentially uncorrelated. On the other hand, the mechanical significance of λ_p is rather that of a length scale: if $L>>\lambda_p$ the polymer will appear easily folded and flexible; conversely, if $L<<\lambda_p$ the polymer will appear very stiff.

Despite the difficulty of directly observing the fluctuations, an estimate of the λ_p can also be provided from the previous values of the bending stiffness. In fact, thinking of the thermal fluctuations as a stochastic force acting on the free polymer, λ_p can also be defined as the length over which the energy of thermal fluctuations is comparable to the elastic energy required to bend a length λ_p of the polymer:

$$\lambda_p = \frac{B}{k_B T}, \tag{4}$$

This definition gives an estimate of $0.4 < \lambda_p < 6$ μm, according to the two extreme values of B deduced in the previous section.

DISCUSSION

In this work, we obtained the equilibrium molecular structures of i-motif DNA nanowires with a repeated $n[(TC_5)_4]$ sequence, by means of MD simulations with the Amber95 force field parametrization. In agreement with the experimental evidence accumulated up to date, such nanowires are assembled by intercalation of the four identical single DNA strands, arranged to give an interplanar distance between basepairs of 0.32 nm, close to the 0.34 nm spacing of B-DNA. To start from a well-defined reference state we always prepared straight structures for our (TC_5) nanowires, a choice consistent with experimental observations. Notably, Guittet et al. (47) reported fully straight intercalated structures for (XC_n) strands with $n \leq 5$, although for $n > 5$ they could observe the formation of more complex structures, staggered and branched into two-dimensional or three-dimensional supramolecular arrangements.

We could confirm the relevant role of the extra proton, resonantly exchanged between coplanar cytosine pairs. In fact, upon MD simulation at T = 300 K and P = 1 atm, the nonprotonated structure was found to be dynamically unstable, whereas the protonated one preserved its structural integrity over the timescale accessible to large-scale MD. Also in good agreement with experimental findings, we observed an alternance along the nanowire of the structure of T•T tetrads. These can be found alternately arranged inward to the cylindrical axis and paired by hydrogen bonds, or freely floating outward to the main axis. Interestingly, it has been suggested that such an alternating behavior of the thymine pairs, which do not appear to accept any extra protons to increase their stability, could be at the basis of a biological switching mechanism (25).

By looking at the ensemble of mechanical properties, namely Young's modulus under uniaxial deformation, the bending stiffness, and the persistence length under three-point bending deformation, we can make a meaningful comparison between the i-motif and other, more common biopolymers (Table 1). First of all, we note that the i-motif appears to belong with the class of structural polymers

TABLE 1 Comparison of some mechanical properties for various biopolymers

	Young's modulus (GPa)	Bending stiffness (Nm[b])	Persistence length (μm)
$n[(TC_5)_4]$ i-motif[a]	1.8 ± 0.5	$(1.9 \pm 0.5) \cdot 10^{-27}$ to $(2.6 \pm 2) \cdot 10^{-26}$	0.4 to 6
F-actin [2]	2.6	$7.3 \cdot 10^{-26}$	17.7
Microtubules (taxol stabilized[b])	1.2	$2.2 \cdot 10^{-23}$	5200
Microtubules (bundles from pillar cells[c])	2	$7 \cdot 10^{-23}$	–
Wool keratin[d]	4	–	–
Single vimentin intermediate filament[e]	0.9 to 2.4	$4 \cdot 10^{-27}$	~1
Elastin[d]	$6 \cdot 10^{-4}$	–	4 to $6 \cdot 10^{-4}$
B-DNA[f]	0.35	$2 \cdot 10^{-28}$	0.05
Chromatin (chicken erythrocite[g])	$7 \cdot 10^{-6}$	–	0.03
Chromosome (mitotic phase[g])	$5 \cdot 10^{-7}$	–	–

[a]This work.
[b]Gittes et al. (41).
[c]Tolomeo et al. (43).
[d]Wainwright et al. (48).
[e]Guzmán et al. (44).
[f]Smith et al. (40).
[g]Marko et al. (49).

(F-actin, microtubules, keratin, etc.), as far as its Young's modulus, although it appears nearly metallic with its tensile strength estimated at >300 MPa. Notably, with its Y in the GPa range, the i-motif is at least one order of magnitude stronger than the DNA strands by which it is made. On the other hand, if we look at its transverse flexibility, as measured by the apparent bending stiffness, the i-motif seems closer to DNA, and one to three orders of magnitudes more flexible than F-actin or microtubules. The reason is that the bending stiffness is mostly determined by the cross section squared, appearing in the second moment of the cross-section I. Compared to F-actin, the i-motif might look similar in terms of Young's modulus, whereas less close in terms of bending. However, the Van der Waals bonded actin monomers are very easily broken apart, compared to the stronger hydrogen bond network of the C•C+ tetrads in the i-motif. Depending on the physiological conditions, F-actin breaks at a force of 230–260 pN (50), which, given its diameter of 5 nm, corresponds to a tensile strength of ~10 MPa, much smaller than the lower limit of 300 MPa we observed for the i-motif. Such a peculiar combination, of a very high tensile modulus and high toughness, and a relatively small bending modulus, makes the i-motif a rather peculiar nanowire from the mechanical point of view: almost inextensible and unbreakable, but quite flexible, somewhat like a nanoscale steel chain. Of course, one should not confuse the tensile strength with the unfolding force, which is reportedly much smaller (51).

By looking again at Table 1, we wish also to underscore the comparison between i-motif, B-DNA, chromatin fiber, and the mitotic chromosome. The tensile stiffness of these objects rapidly decreases, from GPa to kPa, the chromatin and chromosome being extremely soft structures very easily coming apart under quite a small force (per unit cross-section area). It might not be without implications that the small portions of i-motif, possibly contained in the chromosome, should behave like hot spots (for example during the transcription phase, when histone-binding proteins exert strong mechanical forces on the chromatin) concentrating the stress around the much tougher and stiffer sites, but still easily flexible, corresponding to the C-rich fragments of the sequence.

One may ask how much the artificial structures we studied could be relevant to actual biological situations. Repeated C_n sequences have been identified, e.g., the $d(CCAT_2)_n$ from satellite III of human centromeres (52) and $d(CCTA_2)_n$ from telomeres of *Bombyx mori* (53). Their actual folding into tetramers or other structures, investigated by NMR spectroscopy, appears to be influenced in a very important way by the linker sequence: for example, in the centromeric sequence CCT_3ACC, replacing in vitro the T_3A by T_4 leads to a completely different folding behavior (54). Direct observation in vivo of similar folding is more difficult. However, some repeated C-rich sequences of centromeric and telomeric regions have been found to fold into an intramolecular i-motif (3–5). Based on our results, such an occurrence could impart an unusual toughness and rigidity to some regions of the genome. We might speculate about the genetic meaning, or function, of such a possibility. Just for the sake of argument, telomere length in white blood cells has been repeatedly observed to have an inverse correlation with blood pressure (55), it is directly related with loss of elasticity of arterial wall (56), and its shortening is increasingly accepted as a predictive biomarker for cardiovascular disease (57). It is highly speculative to ask whether such an effect in leukocytes could also have a mechanical component, stemming from a higher rigidity of telomere regions, ultimately linked to the possible presence of i-motif structures. If at least partly chromatin integrity could be associated with the presence of long telomeres, one may wonder whether the age-related, progressive shortening of telomeres could also imply the absence of tougher i-motifs segments, someway contributing to cell aging via easier DNA degradation.

CONCLUSIONS

In addition to their potential genetic significance, yet to be fully understood, i-motif nanowires with their peculiar mechanical properties could also represent very good candidates for biomimetic nanoscale templates. As recalled in the Introduction, bioinspired nanowires are high on the wish list of nanotechnology, for their promising potential of easily obtaining tailored and cheap self-assembled, nm-scale structures, onto which other nanometric objects with predesigned functional properties (electric, electronic, magnetic, optical, etc.) could be assembled with a high degree of precision, e.g., via selective ligand-ligand interactions at well-defined sites of the bionanowire. The self-assembled scaffold of i-motif tetramer can be cheaply arranged by design from simple DNA strands, into long-time stable nanowires (8) and two-dimensional or three-dimensional branched structures (47), moreover with highly peculiar mechanical properties, as we showed here. DNA is a common target for antiviral, antibiotic, anticancer drugs, capable of intercalating in the double-helix structure, or adsorbing at the major/minor grooves. Such high ligand selectivity is likely to persist also in the i-motif parent structure, thus making for identification and addressing of preferential target sites: an ideal feature for nanostructure self-assembly. As a relatively flexible, but very stiff and very tough nanostructure at the same time, the i-motif could ideally serve to support structural and functional components in complex nanoscale devices.

SUPPORTING MATERIAL

One table is available at http://www.biophysj.org/biophysj/supplemental/S0006-3495(13)01186-7.

We gladly acknowledge useful discussions with Dominique Collard (LIMMS Cnrs, Tokyo) who first suggested to us to investigate the i-motif structure.

Computing grants from French Supercomputing Center IDRIS, and from CEA-TGCC (in the frame of the PRACE 2010–030294 Project to F.C. and R.B.) are acknowledged. R.P.S. gratefully thanks the President of the University Lille I for a collaborative, three-year PhD grant.

REFERENCES

1. Gehring, K., J.-L. Leroy, and M. Guéron. 1993. A tetrameric DNA structure with protonated cytosine.cytosine base pairs. *Nature.* 363:561–565.
2. Guéron, M., and J.-L. Leroy. 2000. The i-motif in nucleic acids. *Curr. Opin. Struct. Biol.* 10:326–331.
3. Phan, A. T., and J.-L. Mergny. 2002. Human telomeric DNA: G-quadruplex, i-motif and Watson-Crick double helix. *Nucleic Acids Res.* 30:4618–4625.
4. Wang, Y., and D. J. Patel. 1993. Solution structure of the human telomeric repeat d[$AG_3(T_2AG_3)_3$] G-tetraplex. *Structure.* 1:263–282.
5. Phan, A. T., M. Guéron, and J.-L. Leroy. 2000. The solution structure and internal motions of a fragment of the cytidine-rich strand of the human telomere. *J. Mol. Biol.* 299:123–144.
6. Leontis, N. B., J. Stombaugh, and E. Westhof. 2002. The non-Watson-Crick base pairs and their associated isostericity matrices. *Nucleic Acids Res.* 30:3497–3531.
7. Leitner, D., W. Schroeder, and K. Weisz. 1998. Direct monitoring of cytosine protonation in an intramolecular DNA triple helix. *J. Am. Chem. Soc.* 120:7123–7124.
8. Ghodke, H. B., R. Krishnan, …, Y. Krishnan. 2007. The I-tetraplex building block: rational design and controlled fabrication of robust 1D DNA scaffolds through non-Watson-Crick interactions. *Angew. Chem. Int. Ed. Engl.* 46:2646–2649.
9. Laisné, A., D. Pompon, and J.-L. Leroy. 2010. [C7GC4]4 association into supra molecular i-motif structures. *Nucleic Acids Res.* 38:3817–3826.
10. Leroy, J.-L. 2009. The formation pathway of i-motif tetramers. *Nucleic Acids Res.* 37:4127–4134.
11. Spóner, J., J. Leszczynski, …, P. Hobza. 1996. Base stacking and hydrogen bonding in protonated cytosine dimer: the role of molecular ion-dipole and induction interactions. *J. Biomol. Struct. Dyn.* 13:695–706.
12. Spacková, N., I. Berger, …, J. Spóner. 1998. Molecular dynamics of hemiprotonated intercalated four-stranded i-DNA: stable trajectories on a nanosecond scale. *J. Am. Chem. Soc.* 120:6147–6151.
13. Gallego, J., E. B. Golden, …, B. R. Reid. 1999. The folding of centromeric DNA strands into intercalated structures: a physicochemical and computational study. *J. Mol. Biol.* 285:1039–1052.
14. Malliavin, T. E., J. Gau, …, J.-L. Leroy. 2003. Stability of the I-motif structure is related to the interactions between phosphodiester backbones. *Biophys. J.* 84:3838–3847.
15. Malliavin, T. E., K. Snoussi, and J.-L. Leroy. 2003. The NMR structure of [$Xd(C_2)]_4$ investigated by molecular dynamics simulations. *Magn. Reson. Chem.* 41:18–25.
16. Fink, H.-W., and C. Schönenberger. 1999. Electrical conduction through DNA molecules. *Nature.* 398:407–410.
17. Yan, H., S. H. Park, …, T. H. LaBean. 2003. DNA-templated self-assembly of protein arrays and highly conductive nanowires. *Science.* 301:1882–1884.
18. Mao, C., C. E. Flynn, …, A. M. Belcher. 2003. Viral assembly of oriented quantum dot nanowires. *Proc. Natl. Acad. Sci. USA.* 100:6946–6951.
19. Berti, L., A. Alessandrini, and P. Facci. 2005. DNA-templated photoinduced silver deposition. *J. Am. Chem. Soc.* 127:11216–11217.
20. Braun, E., Y. Eichen, …, G. Ben-Yoseph. 1998. DNA-templated assembly and electrode attachment of a conducting silver wire. *Nature.* 391:775–778.
21. Scheibel, T., R. Parthasarathy, …, S. L. Lindquist. 2003. Conducting nanowires built by controlled self-assembly of amyloid fibers and selective metal deposition. *Proc. Natl. Acad. Sci. USA.* 100:4527–4532.
22. Phillips, J. C., R. Braun, …, K. Schulten. 2005. Scalable molecular dynamics with NAMD. *J. Comput. Chem.* 26:1781–1802.
23. Ndlovu, H., A. E. Ashcroft, …, S. A. Harris. 2012. Effect of sequence variation on the mechanical response of amyloid fibrils probed by steered molecular dynamics simulation. *Biophys. J.* 102:587–596.
24. Kästner, J. 2009. Umbrella integration in two or more reaction coordinates. *J. Chem. Phys.* 131:034109.
25. Leroy, J.-L. 2003. T.T pair intercalation and duplex interconversion within i-motif tetramers. *J. Mol. Biol.* 333:125–139.
26. Pettersen, E. F., T. D. Goddard, …, T. E. Ferrin. 2004. UCSF Chimera—a visualization system for exploratory research and analysis. *J. Comput. Chem.* 25:1605–1612.
27. Humprey, W., A. Dalke, and K. Schulten. 1996. VMD: visual molecular dynamics. *J. Molec. Graphics.* 14:33–38.
28. Snoussi, K., S. Nonin-Lecomte, and J.-L. Leroy. 2001. The RNA i-motif. *J. Mol. Biol.* 309:139–153.
29. Privalov, P. L., A. I. Dragan, …, C. A. Minetti. 2007. What drives proteins into the major or minor grooves of DNA? *J. Mol. Biol.* 365:1–9.
30. Feig, M., and B. M. Pettitt. 1999. Sodium and chlorine ions as part of the DNA solvation shell. *Biophys. J.* 77:1769–1781.
31. Bustamante, C., S. B. Smith, …, D. Smith. 2000. Single-molecule studies of DNA mechanics. *Curr. Opin. Struct. Biol.* 10:279–285.
32. Marszalek, P. E., and Y. F. Dufrêne. 2012. Stretching single polysaccharides and proteins using atomic force microscopy. *Chem. Soc. Rev.* 41:3523–3534.
33. Cocco, S., J. F. Marko, and R. Monasson. 2002. Theoretical models for single molecule DNA and RNA experiments: from elasticity to unzipping. *C. R. Phys.* 3:569–584.
34. Ritort, F. 2006. Single-molecule experiments in biological physics: methods and applications. *J. Phys. Condens. Matter.* 18:R531–R583.
35. Cleri, F. 2008. Microscopic mechanics of biomolecules in living cells. *Sci. Model. Simul.* 15:339–362.
36. Manca, F., S. Giordano, …, L. Colombo. 2012. Elasticity of flexible and semiflexible polymers with extensible bonds in the Gibbs and Helmholtz ensembles. *J. Chem. Phys.* 136:154906.
37. Manca, F., S. Giordano, …, L. Colombo. 2012. Theory and Monte Carlo simulations for the stretching of flexible and semiflexible single polymer chains under external fields. *J. Chem. Phys.* 137:244907.
38. Manca, F., S. Giordano, …, L. Colombo. 2013. Two-state theory of single molecule stretching experiments. *Phys. Rev. E Stat. Nonlin. Soft Matter Phys.* 87:032705.
39. Izrailev, S., S. Stepaniants, …, K. Schulten. 1998. Steered molecular dynamics. *In* Computational Molecular Dynamics: Challenges, Methods, Ideas. P. Deuflhard, J. Hermans, B. Leimkuhler, A. E. Mark, S. Reich, and R. D. Skeel, editors. Lecture Notes in Computational Science and Engineering, 4:39–65. Springer-Verlag, Berlin.
40. Smith, S. B., Y. Cui, and C. Bustamante. 1996. Overstretching B-DNA: the elastic response of individual double-stranded and single-stranded DNA molecules. *Science.* 271:795–799.
41. Gittes, F., B. Mickey, …, J. Howard. 1993. Flexural rigidity of microtubules and actin filaments measured from thermal fluctuations in shape. *J. Cell Biol.* 120:923–934.
42. Kis, A., S. Kasas, …, L. Forró. 2002. Nanomechanics of microtubules. *Phys. Rev. Lett.* 89:248101.
43. Tolomeo, J. A., and M. C. Holley. 1997. Mechanics of microtubule bundles in pillar cells from the inner ear. *Biophys. J.* 73:2241–2247.
44. Guzmán, C., S. Jeney, …, L. Forró. 2006. Exploring the mechanical properties of single vimentin intermediate filaments by atomic force microscopy. *J. Mol. Biol.* 360:623–630.

45. Den Otter, W. K., S. H. Shkulipa, and W. J. Briels. 2003. Buckling and persistence length of an amphiphilic worm from molecular dynamics simulations. *J. Chem. Phys.* 119:2363–2368.

46. Gere, J. M., and S. P. Timoshenko. 1999. Mechanics of Materials. Nelson Thornes, Cheltenham, United Kingdom.

47. Guittet, E., D. Renciuk, and J.-L. Leroy. 2012. Junctions between i-motifs in supramolecular structures. *Nucleic Acids Res.* 40:5162–5170.

48. Wainwright, S. A., W. D. Biggs, …, J. M. Gosline. 1976. Mechanical Design in Organisms. Princeton University Press, Princeton, NJ.

49. Marko, J. F., and M. G. Poirier. 2003. Micromechanics of chromatin and chromosomes. *Biochem. Cell Biol.* 81:209–220.

50. Liu, X., and G. H. Pollack. 2002. Mechanics of F-actin characterized with microfabricated cantilevers. *Biophys. J.* 83:2705–2715.

51. Dhakal, S., Z. Yu, …, H. Mao. 2012. G-quadruplex and i-motif are mutually exclusive in ILPR double-stranded DNA. *Biophys. J.* 102:2575–2584.

52. Grady, D. L., R. L. Ratliff, …, R. K. Moyzis. 1992. Highly conserved repetitive DNA sequences are present at human centromeres. *Proc. Natl. Acad. Sci. USA*. 89:1695–1699.

53. Zakian, V. A. 1995. Telomeres: beginning to understand the end. *Science.* 270:1601–1607.

54. Nonin, S., and J.-L. Leroy. 1996. Structure and conversion kinetics of a bi-stable DNA i-motif: broken symmetry in the [d(5mCCTCC)]4 tetramer. *J. Mol. Biol.* 261:399–414.

55. Jeanclos, E., N. J. Schork, …, A. Aviv. 2000. Telomere length inversely correlates with pulse pressure and is highly familial. *Hypertension.* 36:195–200.

56. Wang, Y. Y., A. F. Chen, …, Q. Y. Zhang. 2011. Association of shorter mean telomere length with large artery stiffness in patients with coronary heart disease. *Aging Male.* 14:27–32.

57. Hoffmann, J., and I. Spyridopoulos. 2011. Telomere length in cardiovascular disease: new challenges in measuring this marker of cardiovascular aging. *Future Cardiol.* 7:789–803.